

The Superstructure of Semiconducting SmTe_{2-x}

Seon-Mi Park, So-Jeong Park, and Sung-Jin Kim¹

Department of Chemistry, Ewha Womans University, #120-750, Seoul, Korea

Received February 16, 1998; in revised form May 20, 1998; accepted May 18, 1998

$\text{SmTe}_{1.84}$ was synthesized and the crystal structure was studied by the single-crystal technique. The substructure was isostructural with LaTe_{2-x} , where corrugated rock salt LaTe slabs alternate with planar tellurium square lattices. The substructure of $\text{SmTe}_{1.84}$ is tetragonal anti- Cu_2Sb type and the superstructure is $\sqrt{5} \times \sqrt{5}$ of the tetragonal subcell. The superstructure is tetragonal, with $P4_2/n$ symmetry, $a = 9.709(1)$ Å and $c = 18.007(7)$ Å. There are both ordered and disordered defects in the Te sheet. The superstructure obtained consists of the three possible stable solutions suggested by Lee and Foran, and all three solutions were found in a single crystal. The resistivity dependence on temperature indicates that $\text{SmTe}_{1.84}$ is semiconducting, which seems due to structural modulation. The structural stability of the other phases of SmTe_n ($n = 1-2$) is discussed in terms of temperature and ionic radius ratio. © 1998 Academic Press

INTRODUCTION

Early transition metal dichalcogenides MX_2 ($M =$ early transition metals such as Ta and Nb; $X =$ S, Se, Te) have been extensively studied for their interesting low dimensionality and resulting anisotropic properties (1, 2). In these materials, transition metals are commonly sandwiched in octahedral or trigonal prismatic coordinates in alternating chalcogen layers. Especially, compounds with d^1 electrons such as TaS_2 and NbSe_2 have attracted much attention due to their charge density wave (CDW) instability. In these materials, one electron in the metal d band coupled with the layered structure is known to be the driving force for CDW (3, 4).

However, rare earth dichalcogenides such as DySe_2 are inverse analogies of d^1 compounds, since there is one hole in an otherwise filled chalcogen p band. It is known that there are complex structural modulations in such rare earth metal dichalcogenides, where structural modulations are associated with square chalcogen layers. A series of rare earth polychalcogenides RX_n (R denotes rare earth; X denotes S,

Se, or Te; $n = 2, 2.5,$ or 3) have a common structural motif; that is, distorted rock salt RX slabs are separated by single or double layers of chalcogen X (5–7). Another interesting fact is that commensurate CDWs have been observed in several rare earth diselenides, in which Se–Se dimerization occurred (8). Similar dimerization and ordered vacancies on Se sheet were observed in $\text{RSe}_{1.9}$ ($R =$ Ce, Pr, La) (9, 10). Due to the Se vacancies, the reduction of coordination number of rare earth metal from 9 to 8 going from $\text{PrSe}_{2.0}$ to $\text{PrSe}_{1.9}$ and $\text{PrSe}_{1.8}$ was observed (9). In the mean time, incommensurate ordering was observed in $\text{PrSe}_{1.9}$ and $\text{DySe}_{1.84}$ (9–11).

A structure with undistorted square coordinate tellurium sheets has been reported for two polytellurides, SmTe_3 and Sm_2Te_5 (12). The ditellurides containing the undistorted telluride sheets make these materials 2-dimensional metals. Recently, in RTe_3 , incommensurate CDWs have been observed and the important role of Fermi-surface nesting was implied (13). Recognition of the charge density wave as a driving force for different modulation structures has allowed researchers to understand the structure of these materials (13). Even though resolving the superstructure is essential for understanding the properties of given materials, it is difficult to do that because of weak superstructure reflections and twinning in crystals. Previously, DiMasi *et al.* reported that $\text{SmTe}_{1.9}$ is a semiconductor; however, no evidence of CDW or ordered defect in the crystal structure was found (14).

In this paper, we report the superstructure of $\text{SmTe}_{1.84}$ as determined from an X-ray single-crystal study. The structural diagram of binary rare earth tellurides in the RX_n ($n = 1-2$) series with respect to ionic radius ratio is drawn.

EXPERIMENTAL

During an attempt to prepare ternary telluride, SmTe_{2-x} was obtained from mixtures of Sm chips (Aldrich, 99.9%), Te powder (Aldrich, 99.997%), and Ni powder (Aldrich, 99.99%) in a molar ratio of 2:3:1 with an excess of LiCl (Janssen, 99%) and RbCl (Strem, 99%) as a flux. The reaction mixture was double-sealed in an evacuated quartz tube

¹ Author to whom correspondence should be addressed. E-mail: sjkim@mm.ewha.ac.kr.

and heated at 680°C for 10 days. The heated product was then slowly cooled to room temperature. The product was washed with water to remove the excess flux.

Preliminary examination and data collection were performed with MoK α_1 radiation ($\lambda = 0.71073 \text{ \AA}$) on an Enraf-Nonius diffractometer equipped with an incident beam monochromator graphite crystal. The unit cell parameters and orientation matrix for data collection were obtained from the least-squares refinement, using the setting angles of 25 reflections in the range $22^\circ < 2\theta(\text{MoK}) < 28^\circ$. Intensity data were collected with the ω - 2θ scan technique. The intensities of three standard reflections measured every hour during the data collection showed no significant deviations during the data collection. The initial positions of all atoms were obtained from the direct methods of the SHELXS-86 program (15). The structure was refined by full-matrix least-squares techniques with the use of the SHELXL-93 program (16).

Chemical compositions of the crystals were confirmed by an energy-dispersive X-ray (EDX) spectrometer equipped with a scanning electron microscope (SEM; Philips XL20, EDX-PV9900).

Electrical resistivities of the single crystal were measured using the four-probe method. For resistivity measurement at low temperature, four gold wires were connected to the crystal with silver paste.

RESULTS AND DISCUSSION

Single crystals of SmTe_{2-x} were coffin-lid-like shaped, and platelet-shaped NiTe crystals were detected as a side product. EDX analysis of the coffin-lid-shaped crystals gave a stoichiometry of SmTe_{1.80}, and incorporation of RbCl and LiCl from the flux and Si from the quartz tube were not detected.

A black SmTe_{2-x} crystal was selected and mounted along the *c*-axis for X-ray analysis. The tetragonal cell parameters were related to the tetragonal subcell by $a_{\text{super}} = (a + 2b)_{\text{sub}}$, $b_{\text{super}} = -(2a + b)_{\text{sub}}$, and $c_{\text{super}} = 2c_{\text{sub}}$. Twenty five randomly chosen reflections consistently gave the same superstructure lattice on about 10 crystals. Weissenberg photographs showed consistent superlattice diffractions. The intensities of the superstructure cell were strong enough for the refinement. The observed Laue symmetry and systematic extinctions ($hk0$: $h + k = 2n + 1$, $h00$: $h = 2n + 1$, $00l$: $l = 2n + 1$) were indicative of the space group $C_{4h}^4-P4_2/n$. This space group and the cell dimensions are very similar to those of PrSe_{1.9}. Therefore, this structure was used as the starting model for our refinement. Details of the X-ray data collections and information about the structural determination are given in Table 1.

Once all atoms were located based on the PrSe_{1.9} structure, reasonable isotropic thermal parameters for Sm and Te atoms in the rock salt slabs were obtained, but

TABLE 1
X-ray Structure Refinement for SmTe_{1.84}

Empirical formula	SmTe _{1.84}
Formula weight (g · mol ⁻¹)	385.14
Temperature (K)	293(2)
Wavelength (Å)	0.71073
Crystal system	Tetragonal
Space group	$C_{4h}^4-P4_2/n$
Unit cell dimensions (Å)	$a = 9.709(1)$ $c = 18.008(7)$
Volume (Å ³)	1697.5(7)
Z	20
Density (calculated) (g · cm ⁻³)	7.53
Absorption coefficient (mm ⁻¹)	1.650
$F(000)$	160.80
Crystal size (mm ³)	0.01(1) × 0.02(1) × 0.24(1)
θ range for data collection (deg)	2.26–24.97
Index ranges	$0 \leq h \leq 11$ $0 \leq k \leq 11$ $0 \leq l \leq 21$
Reflections collected	1501 [$R_{\text{int}} = 0.0385$]
Data/restraints/parameters	605/0/80
Goodness-of-fit on F	605/0/80
$R_1 (F_o^2 > 2\sigma(F_o^2))$	5.620%
$wR_2 (F_o^2 > 0)$	11.42%

abnormally large thermal parameters of Te atoms in the Te square sheet were observed. Therefore, the occupancies of Te sites were allowed to vary throughout the balance of the refinement. The occupancy factors for Te(4), Te(5), and Te(6) were 85, 52, and 62%, respectively. The distance between Te(4) and Te(5) was 2.821(8) Å, which indicates a dimerization. Three large peaks remained in the Fourier difference map and two of them were very close to the dimer of Te(4)–Te(5), e.g., 0.67(1) Å from Te(4) and 0.84(2) Å from Te(5), and one of them was on the site isolated from other Te's. Te(7) and Te(8) were assigned to the first two peaks and the occupancies were refined to be 11.9 and 32%, respectively. The isolated peak was assigned as Te(9) and the occupancy factor for Te(9) was refined to be 14%, which is empty in the PrSe_{1.9} structure. No evidence of defect of Te in the rock salt slabs (Te(1), Te(2), and Te(3)) was found. The overall structure and the defect square lattice of Te are shown in Figs. 1 and 2. Atomic coordinates and equivalent isotropic displacement factors are shown in Table 2.

The distance between Te(8) and Te(7) was 2.23(2) Å, which is too short for any Te–Te bond. A dimerization does not likely occur between them; therefore, simultaneous occupation of both sites must be precluded. However, the distance between Te(4) and Te(7) was 2.80(2) Å and the bond distance Te(5)–Te(8) was 2.88(2) Å, which were in the range of bond distance of Te dimers. The relative orientations of Te(4)–Te(7) and Te(5)–Te(8) dimers were similar; e.g., if Te(4)–Te(7) dimer was rotated 162.8(5)° around the origin of

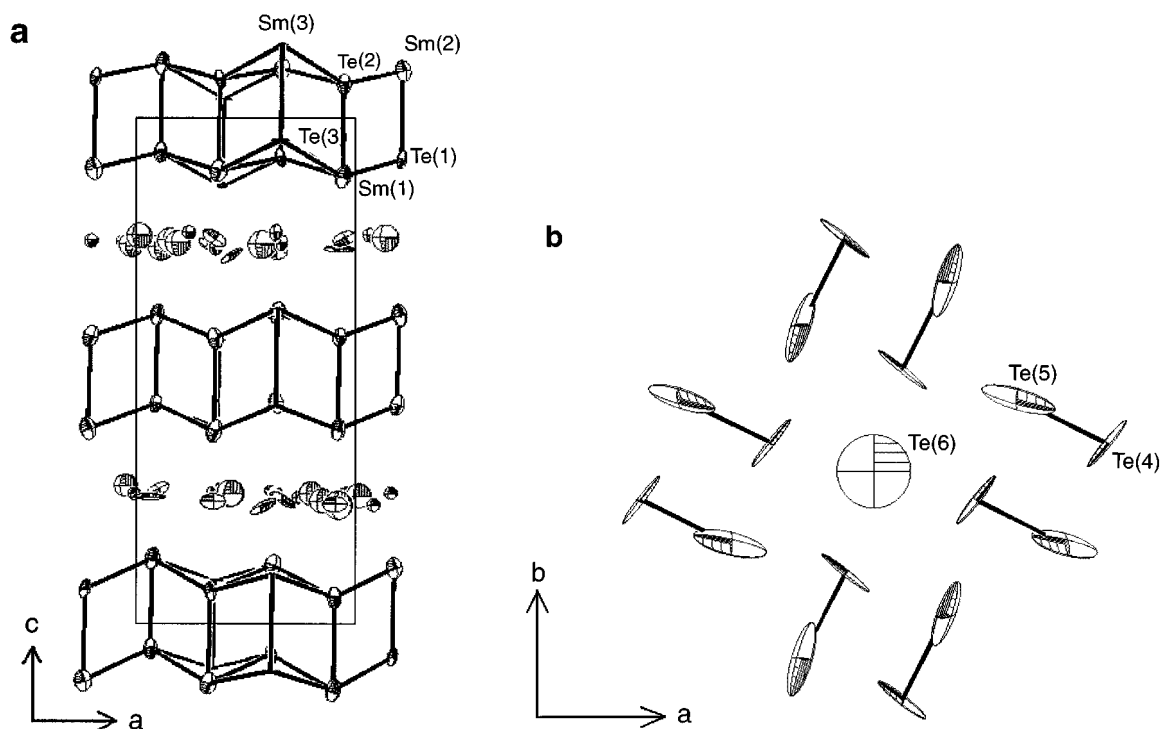


FIG. 1. (a) Structure of SmTe_{1.84}. Thermal ellipsoids (90% probability ellipsoids) of all Te and Sm atoms in rock salt and Te sheets are drawn. In (b) the Te atoms in a single Te layer are drawn with thermal ellipsoids (100% probability ellipsoids). For clarity, Te(7), Te(8), and Te(9) are omitted.

the unit cell, it was overlapped onto Te(5)–Te(8) as shown in Fig. 2. Since the occupancies of Te(4), Te(5), and Te(7) were quite different, the possibility of forming trimers was excluded. For clarity, only the relative orientations of Te(4)–Te(5) and Te(4)–Te(7) dimers are presented in Figs. 2b and 2c.

The average Te–Te bond distance in the Te sheet was 3.02 Å, which is in the range of metallic Te–Te bond distance and comparable with those of SmTe₃ and Sm₂Te₅. The average distance of Te–Te dimers was 2.83 Å and the distance between Te dimers and monomers Te₂²⁻–Te²⁻ was 3.10 Å, which were shorter than those in the stoichiometric SmTe_n (*n* = 2, 2.5, 3). The occupancy of Te(6) was refined to be 62%, which is quite different from the corresponding selenium position in PrSe_{1.9} that is fully occupied. Therefore, there are disordered vacancies on Te sheets. Finally, refined occupancies gave the stoichiometry of SmTe_{1.84}. Atomic coordinates, thermal factors, occupation factors, and the important distances are reported in Tables 2, 3, and 4.

Assuming Sm³⁺ and Te²⁻ to be the atoms in the rock salt layers, the average charge on each of Te atoms in the defective square lattice was $-10/8.4 = -1.19$. This average charge was the same as that of the selenide analog

DySe_{1.84} (11). The defective Te layers were built up by isolated Te and dimerized Te–Te and their oxidation states could be assigned as Te²⁻ and (Te–Te)²⁻, respectively. When Te(6) and Te(9) were assigned to be Te²⁻ and Te(4), Te(5), Te(7), and Te(8) to be Te¹⁻, the best charge balance was obtained. Since overall composition and charge balance corresponded to Sm₁₀Te₁₀(Te_{1.2})²⁻(Te_{7.2})¹⁻, there were approximately three dimers for every monomer. Considering the occupancy factors, the coordination numbers of Sm were between 7 and 9; e.g., the coordination numbers for Sm(1), Sm(2), and Sm(3) were 8.18, 7.73, and 8.38, respectively. In the selenium analog PrSe_{1.9}, the coordination numbers for Pr(1) and Pr(2) are 9 and the coordination number for Pr(3) is 8.

With the composition established, data were corrected for absorption using the analytical ψ -scan method. Anisotropic thermal motions were included (Table 3); however, Te(7), Te(8), and Te(9) were refined only isotropically because of their low occupancies. Some features in thermal ellipsoids were observed (Fig. 1). The thermal ellipsoids of Sm(1), Sm(2), Te(1), and Te(2) were elongated along the *c*-axis. However, Sm(3)-bounded Te(3) have pancake-shaped thermal ellipsoids in the *ab* plane direction (Fig. 1b). Telluriums in the Te sheet, Te(4), Te(5), and Te(6), commonly have

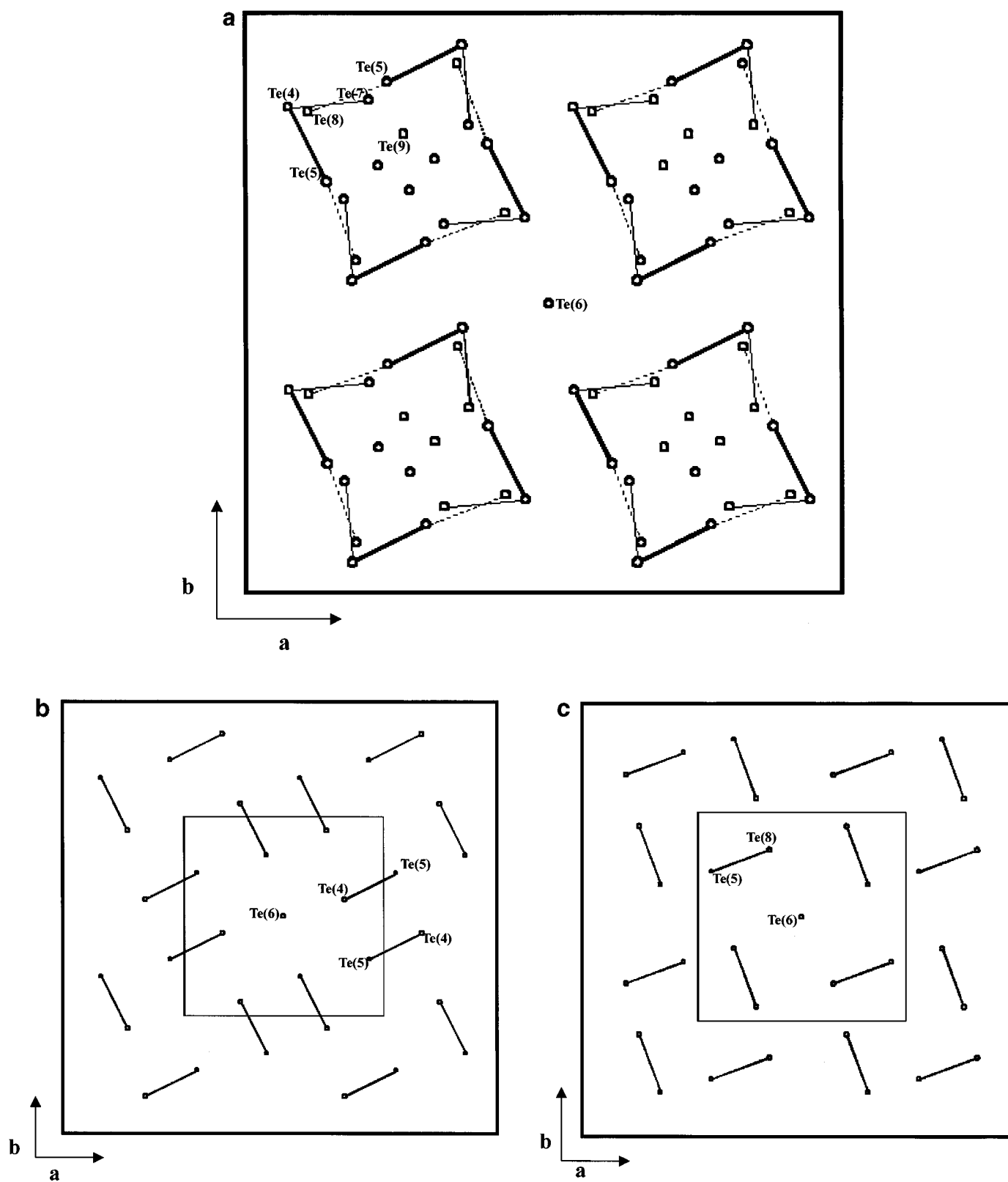


FIG. 2. (a) Experimentally determined features of the defective square lattice of $\text{SmTe}_{1.84}$. The thick solid lines, thin solid lines, and dotted lines illustrate Te(4)-Te(5), Te(4)-Te(7), and Te(5)-Te(8) dimers, respectively. (b) Only the orientation of Te(4)-Te(5) dimers with the $\sqrt{5} \times \sqrt{5}$ unit cell is presented. (c) Only the orientation of Te(4)-Te(7) dimers with the $\sqrt{5} \times \sqrt{5}$ unit cell is presented.

TABLE 2
Atomic Coordinates and Equivalent Isotropic Displacement Factors $U_{(eq)}$ (\AA^2) for $\text{SmTe}_{1.84}$

Atom	Position	<i>x</i>	<i>y</i>	<i>z</i>	Occupancy (%)	$U_{(eq)}^a$
Sm1	8g	0.9524(4)	0.6474(3)	0.1189(1)	100	0.0159(7)
Sm2	8g	0.1490(3)	0.0495(4)	0.1107(1)	100	0.0149(7)
Sm3	4e	0.7500	0.2500	0.1148(2)	100	0.005(1)
Te1	8g	0.5493(5)	0.8500(4)	0.4319(1)	100	0.0101(8)
Te2	8g	0.1504(4)	0.0503(6)	0.4385(1)	100	0.0137(8)
Te3	4e	0.7500	0.2500	0.4337(2)	100	0.007(2)
Te4	8g	0.0559(4)	0.8350(6)	0.2503(3)	85(2)	0.014(1)
Te5	8g	0.3200(8)	0.9672(7)	0.2509(5)	52(1)	0.018(1)
Te6	2b	0.2500	0.2500	0.7500	62(1)	0.028(3)
Te7	8g	1.118(2)	0.467(2)	0.242(1)	11.9(9)	0.0157(1) ^b
Te8	8g	1.076(1)	0.906(2)	0.254(1)	32(2)	0.039(6) ^b
Te9	8g	1.243(3)	0.349(2)	0.255(1)	14(1)	0.039(1) ^b

^a $U_{(eq)}$ is defined as one third of the orthogonalized U_{ij} tensor.

^b $U_{(iso)}$.

pancake-shaped thermal ellipsoids in the *ab* plane. These abnormal ellipsoids are found in other series of non-stoichiometric compounds such as $\text{DySe}_{1.84}$ and $\text{YSe}_{1.83}$ (11, 17) and these seem to be real features, not artificial ones due to a fault in the absorption correction. The final cycle of refinement was performed on F_o^2 with 1501 unique reflections, and it gave residuals of $wR_2(F_o^2 > 0) = 11.42\%$; the conventional *R* index based on the reflections having $F_o^2 > 2\sigma(F_o^2)$ was 5.62%. The difference Fourier synthesis calculated with the phases based on the final parameters showed no peak greater than 0.6% of the height of a Te atom. Low-symmetry space groups such as $P4_2$, $P\bar{4}$ and $P2/n$ were tested, but their *R* values were significantly unfavorable.

TABLE 3
Anisotropic Displacement Parameters (\AA^2) for $\text{SmTe}_{1.84}^a$

Atom	U_{11}	U_{22}	U_{33}	U_{23}	U_{13}	U_{12}
Sm(1)	0.009(1)	0.013(1)	0.025(1)	0.004(1)	-0.001(1)	-0.001(1)
Sm(2)	0.012(1)	0.009(1)	0.023(1)	0.0006(1)	0.001(1)	0.001(0)
Sm(3)	0.009(2)	0.007(2)	0.000(1)	0	0	-0.003(1)
Te(1)	0.005(1)	0.009(1)	0.016(1)	-0.0003(1)	-0.0024(1)	-0.0009(1)
Te(2)	0.010(1)	0.001(1)	0.022(1)	-0.0031(1)	-0.0011(1)	0.002(1)
Te(3)	0.013(2)	0.009(3)	0.000(2)	0	0	0.002(1)
Te(4)	0.015(1)	0.018(3)	0.011(1)	0.0007(1)	0.0003(2)	-0.015(2)
Te(5)	0.038(1)	0.007(3)	0.011(3)	-0.0007(2)	-0.016(3)	0.010(2)
Te(6)	0.042(5)	0.042(5)	0.000(3)	0	0	0
Te(7)	0.0157(1)					
Te(8)	0.039(5)					
Te(9)	0.039(1)					

^aThe anisotropic displacement factor exponent takes the form

$$-2\pi^2(h^2a^{*2}U_{11} + \dots + 2hka^*b^*U_{12}).$$

TABLE 4
Interatomic Distances (\AA) for $\text{SmTe}_{1.84}$

Sm(1)-Te(1)	3.213(3), 3.232(3)
-Te(2)	3.218(3), 3.253(3)
-Te(3)	3.206(2)
-Te(4)	3.177(3), 3.295(3)
-Te(5)	3.470(3)
-Te(6)	3.226(2)
-Te(7)	3.28(2)
-Te(8)	3.17(2)
Sm(2)-Te(1)	3.150(3), 3.292(3)
-Te(2)	3.189(3), 3.201(3)
-Te(3)	3.176(2)
-Te(4)	3.388(4)
-Te(5)	3.150(3), 3.292(3)
-Te(7)	2.95(2), 3.26(2)
-Te(8)	3.02(2)
-Te(9)	3.01(2), 3.02(2)
Sm(3)-Te(1)	3.182(4) (2 ×)
-Te(2)	3.226(6) (2 ×)
-Te(3)	3.248(4)
-Te(4)	3.165(3) (2 ×)
-Te(5)	3.235(2) (2 ×)
-Te(8)	3.30(4) (2 ×)
Te(4)-Te(5)	2.821(8), 3.171(2)
-Te(6)	3.098(3)
-Te(7)	2.80(2)
Te(5)-Te(7)	3.17(2)
-Te(8)	2.88(2)
-Te(9)	3.12(2)
Te(7)-Te(8)	3.20(3)
-Te(9)	2.97(3)
Te(8)-Te(9)	3.00(4)

In selenium compounds such as LaSe_2 and CeSe_2 , initial square sheets were distorted to generate Se_2^{2-} dimers forming a 1×2 superstructure (17). Previously, the energetic stability of Se_2^{2-} dimers and their relative orientation of herringbone pattern were rationalized by Lee and Foran, based on the second-moment scaled Hückel theory (18). The result of similar calculations for the $\text{LaSe}_{1.9}$ -type structure gave three possible superstructures with $\sqrt{5} \times \sqrt{5}$ of subcell in the *a, b* direction. In this model, the Se square consists of four Se_2^{2-} dimers per Se^{2-} monomer as a result of displacive ordering of Se and defects of 1/10 selenium atom per unit cell, and this agreed with the experimentally observed superstructure of $\text{PrSe}_{1.9}$ (9).

A structure with undistorted square coordinate chalcogen sheets in rare earth tellurides has been reported (5,6,12). However, in this research, dimerization of telluriums and complicated defects in the Te sheet were observed. The lattice parameters *a* and *c* of the title compound decreased relative to those of stoichiometric ditellurides, as observed

in $\text{NdTe}_{1.8}$. As in other polychalcogenides such as SmTe_3 and Sm_2Te_3 , each Sm and Te in the rock salt slabs had five corresponding Te and Sm neighbors in $\text{SmTe}_{1.84}$. According to a previous calculation performed on $\text{La}_{10}\text{Se}_{19}$ (18), the relative orientation of Te(4)–Te(5)-type dimers is the most stable solution and Te(4)–Te(7)-type dimerization is the second most stable solution in terms of covalent and total energy. The main difference between Te(4)–Te(5) and Te(4)–Te(7) dimer orientation is the ionic energy caused by repulsion between Te_2^{2-} dimer and Te^{2-} monomer. If Te(6) is fully occupied, then the repulsion interaction between Te^{2-} (Te(6)) and Te_2^{2-} (Te(4)–Te(7)) would destabilize Te(4)–Te(7)-type dimerization. However, since Te(6) is only partially occupied, the stability of Te(4)–Te(7)-type dimerization is comparable with Te(4)–Te(5)-type dimerization. This is the first case in $R\text{Te}_n$ -type ($n = 2, 2.5, 3$) tellurides where the suggested superstructure model expected from the calculation was actually observed. Furthermore, the two most stable models were observed to coexist in a single crystalline.

The resistivity measured from a single crystal increased as temperature decreased, showing that this crystal is semiconducting (Fig. 3). The band gap calculated in the range 100–250 K was 0.04 eV. Previously, metallic properties were found in SmTe_3 and Sm_2Te_5 (12). However, a semiconducting property in $\text{SmTe}_{1.9}$ with large anisotropic transport properties was observed by DiMasi *et al.* (14). The result of our resistivity measurement was similar to that of DiMasi *et al.* (14). Based on our structural investigation, bond-breaking distortion in the Te square sheets seemed to lead the semiconducting state.

Going from SmTe_3 to Sm_2Te_5 , SmTe_2 , $\text{SmTe}_{1.9}$, and $\text{SmTe}_{1.8}$, there was a successive reduction in the compounds. In this series of compounds, there was an electron transfer from Sm in the rock salt layer to the square Te layers. Therefore, there is an increase in the electron concen-

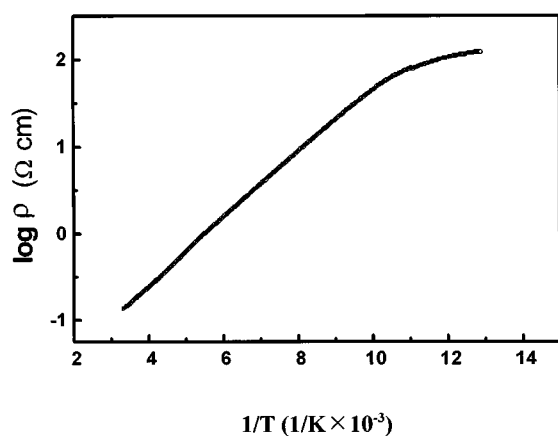


FIG. 3. Logarithmic electrical resistivity vs inverse temperature for $\text{SmTe}_{1.84}$.

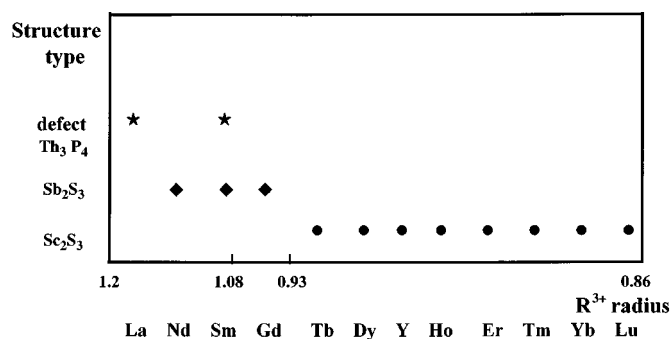


FIG. 4. Field map of $R_2\text{Te}_3$ structure type and R^{3+} . Radii of cations in angstroms are estimated each structure type.

tration in the p band of the Te sheets with successive reduction of these compounds. Some of the factors affecting the CDW instability are known to be the electron concentration on Te, the relative size of the cation and anion, and the polarizability of the chalcogen. Since $\text{SmTe}_{1.84}$ is obtained only in the limit of maximum x in SmTe_{2-x} , the observed lattice distortions in $\text{SmTe}_{1.84}$ and induced semiconducting behavior seemed mainly due to their high electron concentration in the Te sheet.

In an attempt to prepare SmTe_{2-x} , Sm_2Te_3 with Sb_2S_3 type was obtained. It is known that rare earth chalcogenides $R_2\text{Te}_3$ have one of three structure types, Th_3P_4 , Sb_2S_3 , and Sc_2S_3 . The limits of the stability may be understood qualitatively in terms of the size of R^{3+} and the synthetic temperature. Figure 4 shows structural types depending on the R^{3+} radius (19a–h). We found that in the composition limit of SmTe_{2-x} , Sm_2Te_3 could be formed with two structures. At low temperature (lower than 700°C), it crystallized with the Sb_2S_3 -type structure and at high temperature (higher than 1000°C), it crystallized with the Th_3P_4 -type structure.

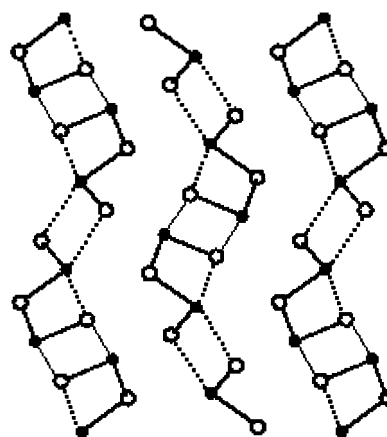


FIG. 5. Sb_2S_3 -type structure. Solid circles are metals and open circles are nonmetals. Bond distances are illustrated by thick solid lines ($d < 3.0 \text{ \AA}$), thin solid lines ($3.0 < d < 3.2 \text{ \AA}$), and dotted lines ($3.2 < d < 3.4 \text{ \AA}$) according to the strength of the interactions.

The structure of Th_3P_4 is a three-dimensionally condensed CsCl-type structure, where each metal is coordinated by 8 nonmetals. The structure of Sb_2S_3 reveals that the chemical bonding can be either 3.0 or 3.4 Å, where the metals are coordinated by 3 or 5 and 5 or 6 sulfurs, respectively. Considering three sulfur coordinates, the structure of Sb_2S_3 consists of chains; however, there were strong interactions (~ 3.4 Å) between two chains to form layers (Fig. 5). Since Te has a strong covalency, Sm_2Te_3 can be described as 2-dimensional layers basically consisting of the rock salt unit. In terms of continuous reduction from SmTe_2 to SmTe_{2-x} , coordination numbers of Sm were reduced from 8 and 9 to 7 and 8 due to the defect of Te of the Te sheet. When the structure of titled SmTe_{2-x} is compared with that of Sb_2S_3 -type Sm_2Te_3 , square tellurium layers of SmTe_{2-x} are totally missing in Sm_2Te_3 and only the rock salt fragments remain. In the Sb_2S_3 structure, the reduction of SmTe_2 seemed to be complete.

ACKNOWLEDGMENTS

This work was supported by the fund BSRI-96-3413 and partly by Advanced Material 1996 from the Korean Ministry of Education.

REFERENCES

1. J. E. Rouxel, "Crystal Chemistry and Properties of Materials with Quasi-One-Dimensional Structure." Reidel, Dordrecht, Holland, 1986.
2. M. S. Whittingham, A. J. Jacobson, and S. Mahajan, "Intercalation Chemistry." Academic, New York, 1982.
3. J. A. Wilson, F. J. DiSalvo, and S. Mahajan, *Adv. Phys.* **24**, 117 (1975)
4. M.-H. Whang and E. J. Canadell, *J. Am. Chem. Soc.* **114**, 9587 (1992).
5. R. Wang, H. Steinfink, and W. F. Bradley, *Inorg. Chem.* **5**, 142 (1966).
6. R. Wang and H. Steinfink, *Inorg. Chem.* **6**, 1685 (1967).
7. M.-P. Pardo and J. Flahaut, *Bull. Soc. Chim. Fr.* **10**, 3658 (1967).
8. S. Benazeth, D. Carre, and P. Laruelle, *Acta Crystallogr., Sect. B* **38**, 33 (1982).
9. P. Plambeck-Fischer, W. Abriel, and W. Urland, *J. Solid State Chem.* **78**, 164 (1989).
10. M. Grupe and W. Urland, *J. Less-Common Met.* **170**, 271 (1991).
11. B. Foran, S. Lee, and M. C. Aronson, *Chem. Mater.* **5**, 974 (1993).
12. E. DiMasi, M. C. Aronson, B. Foran, S. Lee, *Chem. Mater.* **6**, 1867 (1994).
13. (a) E. DiMasi, M. C. Aronson, J. F. Mansfield, B. Foran, and S. Lee, *Phys. Rev. B* **52**, 14516 (1995); (b) S. Lee and B. Foran, *J. Am. Chem. Soc.* **118**, 154 (1996).
14. E. DiMasi, M. C. Aronson, B. Foran, and S. Lee, *Physica B* **206&207**, 386 (1995).
15. G. M. Sheldrick, *Acta Crystallogr., Sect. A* **46**, 467 (1990).
16. G. M. Sheldrick, SHELXL 93, Program for the Refinement of Crystal Structure, University of Gottingen, Gottingen, Germany, 1993.
17. S.-J. Kim and H.-J. Oh, *Bull. Korean Chem. Soc.* **16**, 515 (1995).
18. S. Lee and B. Foran, *J. Am. Chem. Soc.* **116**, 154 (1994).
19. (a) W. L. Cox, H. Steinfink, and W. F. Bradley, *Inorg. Chem.* **5**, 318 (1966); (b) W. Lin, H. Steinfink, and E. J. Weiss, *Inorg. Chem.* **4**, 877 (1965); (c) J. P. Dismukes and J. G. White, *Inorg. Chem.* **4**, 970 (1965); (d) D. J. Haase, H. Steinfink, and E. J. Weiss, *Inorg. Chem.* **4**, 541 (1965); (e) J. Flahaut, L. Domange, M. Guittard, and M. P. Pardo, *Bull. Soc. Chim. Fr.* 326 (1965); (f) J. Flahaut, P. Laruelle, M. P. Pardo, and M. Guittard, *Bull. Soc. Chim. Fr.* 1399 (1965); (g) J. S. Swinnea, H. Steinfink, and L. R. Danielson, *J. Appl. Crystallogr.* **20**, 102 (1987); (h) V. K. Slovyanskikh, N. T. Kuznetsov, and N. V. Gracheva, *Russ. J. Inorg. Chem.*, **30**, 1077 (1985).